A C-terminal amphipathic helix is necessary for the *in vivo* tubule-shaping function of a plant reticulon

Emily Breeze[1], Natasha Dzimitrowicz[1], Verena Kriechbaumer[4], Rhiannon Brooks[2], Stanley W. Botchway[3], Jacob P. Brady[5], Chris Hawes[4], Ann Dixon[2], Jason R. Schnell[5], Mark D. Fricker[6] and Lorenzo Frigerio[1,*]

[1]School of Life Sciences and [2]Department of Chemistry, University of Warwick, Coventry CV4 7AL, United Kingdom
[3] Central Laser Facility, Science and Technology Facilities Council (STFC) Rutherford Appleton Laboratory, Research Complex at Harwell, Didcot OX11 0QX, United Kingdom
[4] Plant Cell Biology, Biological and Medical Sciences, Oxford Brookes University, Oxford OX3 0BP, United Kingdom
[5]Department of Biochemistry, University of Oxford, Oxford OX1 3QU, United Kingdom
[6]Department of Plant Sciences, University of Oxford, Oxford OX1 3RB, United Kingdom

* corresponding author

Running title: Novel structural features of a plant reticulon

Keywords: Amphipathic helix/endoplasmic reticulum/reticulon/plant

Character count:

Classification: Biological Sciences; Cell Biology

Abstract

Reticulons (RTN) are a class of endoplasmic reticulum (ER) membrane proteins that are capable of maintaining high membrane curvature, thus helping shape the ER membrane into tubules. The mechanism of action of RTNs is hypothesised to be a combination of wedging, resulting from the transmembrane topology of their conserved reticulon homology domain, and scaffolding, arising from the ability of RTNs to form low-mobility homo-oligomers within the membrane. We have studied the plant RTN isoform RTN13, which has previously been shown to locate to ER tubules and the edges of ER cisternae and to induce constrictions in ER tubules when overexpressed, and have identified a region in the C-terminus containing a putative amphipathic helix (APH). Here we show that deletion of

this region or disruption of the hydrophobic face of the predicted helix abolishes the ability of RTN13 to induce constrictions of ER tubules *in vivo*. These mutants, however, still retain their ability to interact and form low-mobility oligomers in the ER membrane. Hence, our evidence indicates that the conserved APH is a key structural feature for RTN13 function *in vivo* and we propose that RTN, like other membrane morphogens, rely on APHs for their function.

Significance Statement

To our knowledge, this is the first *in vivo* demonstration that reticulon (RTN) proteins, responsible for the shaping and maintenance of ER membrane tubules, rely on a highly conserved C-terminal amphipathic helix (APH) for their morphogenic function. Previously it was thought that RTN could bend the ER membrane both by assuming a wedge-like topology and by forming oligomeric arcs. We show here that deleting or mutating the APH region abolishes the function of a plant RTN, but does not affect its capacity to oligomerise. This indicates that proteins of the RTN family use an APH to affect membrane curvature – a mechanism that is shared by several other membrane-shaping protein families.

Introduction

As the gateway to the secretory pathway, the endoplasmic reticulum (ER) is responsible for secretory protein translocation, folding and quality control, and is thus central to the maintenance of cellular homeostasis (1). In plant cells, the ER consists of the nuclear envelope and a dynamic peripheral network of cisternae and, more predominantly, tubules extending throughout the cytoplasm and across cell boundaries through plasmodesmata. Several proteins have been implicated in the shaping of the ER membrane. In plants these include ROOT HAIR DEFECTIVE3 (RHD3), which is orthologous to mammalian atlastins and yeast Sey1p and is likely important for the formation of three-way junctions (2, 3), and the proteins of the reticulon (RTN) family. The RTNs are preferentially associated with ER tubules and the curved edges of

cisternae. When overexpressed *in planta*, RTNs induce severe constrictions of ER tubules and are able to convert ER membrane sheets into tubules (4-6).

The mechanism by which RTNs generate and/or stabilize curvature of a membrane has been attributed to the reticulon homology domain (RHD)— a conserved domain of ~200 amino acids containing two long hydrophobic regions flanking a hydrophilic loop. These two hydrophobic regions can each be further subdivided into two transmembrane domains (TMDs), resulting in a 'W' – like topology. The RHD is also found in the DP1 (deleted in polyposis) family of proteins that includes Yop1p in yeast and human REEPs (receptor expression-enhancing proteins). The four hydrophobic TMDs of the plant RHD are proposed to form wedge-like hairpins in the lipid bilayer, which, in combination with the RHD-mediated oligomerisation of RTNs into low-mobility oligomers, appear to be sufficient to induce membrane curvature (5-9). We have previously shown that shortening of three or all four TMDs of the Arabidopsis reticulon RTNLB13 (Reticulon-like protein B13; henceforth referred to as RTN13) results in the protein losing its ability to induce tubules, form oligomers, and localise to high-curvature membranes (5, 6). Interestingly, Zurek et al. (10) observed a similar loss of membrane-shaping function and tubule partitioning through extending the length of TMDs of human RTN4. These results indicate that the precise length of the hydrophobic hairpins is critical for RTN functionality, possibly by allowing the formation of homo-oligomers (7).

Recently, Brady et al. (11) used solution NMR of lipid- and detergent-containing micelles of recombinant Yop1p to gain structural insights in this class of ER tubule-shaping proteins. They identified a novel structural motif, an amphipathic helix (APH) in Yop1p. This APH is located in the C-terminal region of the protein, near the C-terminal end of the fourth TMD, and appears to be highly conserved across all RTN family proteins. Notably, an isolated peptide of the Yop1p APH was seen to interact strongly with anionic membranes and, while the native Yop1p protein can induce tubule formation when reconstituted into polar lipids *in vitro*, a truncated version of Yop1p lacking the APH was unable to do so (9, 11). C-terminal cytosolic APHs have also been identified and characterized in other membrane shaping proteins, including atlastin, in which the APH was shown to facilitate the destabilization of the lipid bilayer to aid membrane fusion and three-way junction formation (12, 13).

We have identified such an APH in the C-terminal region of RTN13, one of the shortest RTN isoforms in Arabidopsis and our model protein for the plant RTN family (4-6). Here

we show that this predicted APH, while not required for oligomer formation, is essential for the membrane-shaping function of RTN13 *in vivo*. Deletion of the APH or disruption of its hydrophobic face results in a loss of tubule-forming activity *in vivo* but does not affect the ability of the protein to form homotypic interactions, or to localize to the ER.

Results and Discussion

Arabidopsis has 21 predicted RTN proteins, of which RTN13 is one of the smallest (206 amino acids), consisting of the RHD plus short N- and C-terminal extensions. We have previously shown that RTN13 is localized to the tubular cortical ER and, when ectopically expressed, is capable of inducing constrictions in ER tubules and to convert ER sheets into tubules, as demonstrated for other, longer RTN isoforms (4-6). As such, RTN13 can be considered to be the minimal functional plant RTN protein, and is thus a useful model for studying the relationship between the structural motifs and topology of RTNs, and their ER morphogenic properties.

To investigate if an APH akin to the one identified in Yop1p (11) was conserved in plant RTNs, analysis of the amino acid sequence of RTN13 was performed. This identified a region of high helical hydrophobic moment (residues E160-K175; Fig 1A-C) which, when plotted as a function of its hydrophobicity, localised to the region occupied by membrane surface-seeking proteins (14) (Fig. 1D). As with Yop1p, the APH is C-terminal to the four predicted TMDs (Fig. 1, A-B). The amphipathic character of this region is a highly conserved feature across many eukaryotic RTN family proteins (Fig. 1D and (11)).

The secondary structure of a synthetic 16 amino acid peptide derived from this putative APH sequence (residues 160-175) was investigated in increasing concentrations of the zwitterionic detergent n-dodecylphosphocholine (DPC) using circular dichroism (CD) spectroscopy. The peptide was readily soluble in aqueous buffer but adopted a random coil secondary structure as evidenced by the single negative maximum in the CD spectrum just below 200 nm (Fig 2, dashed line). Addition of increasing concentrations of DPC from 10-200 mM lead to a steady reduction in the peak corresponding to random coil secondary structure, and the emergence of negative maxima centred at approximately 208 and 222 nm, characteristic of α-helical secondary structure. These data indicate that this region of RTN13 has a propensity to associate with DPC micelles, used here as a rough model for phosphatidylcholine membranes, and that this association initiates α-helix formation, thus supporting the presence of a membrane-

associated APH.

To establish if the presence of the predicted APH is required *in vivo* for the ER membrane remodeling phenotype induced by overexpression of RTN13, we first generated C-terminal truncations of RTN13, tagged at the N-terminus with YFP (4), by inserting a stop codon immediately prior to the predicted APH (Δ160-206; Fig. 1E), and by excising the sequence encoding the predicted APH (ΔAPH; Fig. 1E).

When co-expressed transiently in *Nicotiana benthamiana* epidermal cells with the ER luminal marker, GFP-HDEL, all mutants retained their ability to localize to tubular ER (Fig. 3). Overexpression of full length YFP-RTN13 caused the typical, marked constriction of ER tubules (Fig 3A), as previously reported. Tubule constrictions displace the luminal marker to discrete, punctate regions of the ER network, thereby resulting in a significant reduction in the degree of colocalisation of GFP-HDEL with YFP-RTN13 (Fig. 3E). Deletion of the APH plus C-terminal region (Δ160-206) and of the region encoding the APH alone (ΔAPH) abolished this phenotype (Fig. 3B, 3D) such that the luminal marker GFP-HDEL colocalised with the tagged RTN13 throughout the ER network (Fig. 3E), indicating that these mutants, while correctly locating to the ER, are incapable of inducing constrictions.

To further investigate if the putative APH alone was solely responsible for the protein's tubule forming capacity, an isoleucine residue in the centre of the predicted hydrophobic face of the APH was mutated to a lysine residue (I165K). This mutation introduces a positive charge within the hydrophobic region of the APH, which decreases the magnitude of the hydrophobic moment by a third relative to wild-type, effectively abolishing amphipathicity in the helix (Fig. 1C). The ER tubule constriction phenotype was not observed upon transient expression of this construct (Fig. 3C). The steady-state protein expression levels of ΔAPH were comparable to full length YFP-RTN13, whereas I165K and Δ160-206 mutant protein expression was slightly lower (Supplemental Fig. 1A). Infiltration with serial dilutions of *Agrobacterium tumefaciens* (OD_{600}) carrying full length YFP-RTN13, which resulted in progressively lower amounts of detectable protein (Supplemental Fig. 1B), did not affect the appearance of the ER constriction phenotype even at the lowest agrobacterial titre (Supplemental Fig. 1C). Thus, we conclude that this phenotype is unlikely to be a function of subtle differences in the protein concentrations achieved within our standard agroinfiltration procedure.

Taken together, these data indicate that the presence of an intact C-terminal APH is

necessary for the membrane-shaping activity of RTN13 *in vivo*.

In addition to the tubule constriction phenotype shown in Fig. 3, we attempted to assess the effect of full-length RTN13 and of the APH mutants on the diameter of ER tubules. We imaged the ER lumen (labelled by GFP-HDEL) in the presence of either full-length or mutated YFP-RTN13, using the Airyscan detector of a Zeiss LSM 880 confocal microscope, which is able to achieve a lateral resolution of around 140 nm. We collected images from 10 expressing cells per construct (representative images are shown in Fig. 4A, left-hand panels), and subjected each image to network analysis. The tubular ER network was automatically extracted to give a single-pixel-wide skeleton. The local image intensity normal to the skeleton was integrated to provide an estimate of the relative amount of GFP-HDEL present for every point along each tubule. Each integrated intensity profile was then scanned to detect intensity peaks, corresponding to bulges in the tubules, and intensity troughs, corresponding to constriction sites (Fig. 4A, right-hand panels). Although the tubules are at or below the resolution limit, the relative intensities can be used as a proxy for the width of the ER tubules, with the additional assumption that GFP-HDEL is evenly distributed in the ER lumen.

We thus estimated the width of the tubules in unperturbed ER (GFP-HDEL alone) and in the presence of full-length or mutated YFP-RTN13. Our analysis showed that constrictions can be regularly detected even in unperturbed ER tubules (Fig. 4A, bottom panel; Fig. 4B). However, we observed that, in the presence of full-length YFP-RTN13, the mean tubule width and the width at the constriction sites were significantly narrower than in unperturbed ER (Fig. 4B). In contrast, in the presence of the RTN13 APH mutants, the mean width of the ER tubules was not significantly different to that observed in the unperturbed network. These data indicate that ectopic expression of RTN13 negatively affects the width of ER tubules and that this property requires the presence of an APH.

Since the RTN proteins are known to form both hetero- and homo-oligomers, which create immobile, arc-like scaffolds in the tubular ER membrane, it is possible that the removal or mutation of the APH affects the ability of RTN13 to oligomerise. Previous work indicated that altering the length of the TMDs within the RHD abolished RTN function, but this was concomitant with a loss of the protein's capacity to homo-oligomerise (5). To test whether our APH mutants had similarly lost the ability to form low mobility homo-oligomers and/or to interact with wild-type RTN13, we used sucrose sedimentation velocity gradients, fluorescence recovery after photobleaching (FRAP)

analysis and Förster resonance energy transfer (FRET), measured directly by fluorescence lifetime imaging (FLIM).

We isolated microsomes from agroinfiltrated *N. benthamiana* leaves, solubilized the membranes with 1% digitonin and resolved the extracts on a continuous 5-30% sucrose gradient, with comparison against known molecular weight marker proteins. Fractions were analysed by SDS-PAGE and immunoblotted with anti GFP antiserum. Fig. 5 shows that both full length YFP-RTN13 and the APH mutants form high molecular weight oligomeric complexes that have comparable sedimentation properties, peaking around a molecular mass of ~200-250 kD. This indicates that these complexes may contain 4-5 monomers, which is comparable to that observed for yeast and mammalian reticulons (7).

FRAP of a region of the tubular ER expressing YFP-RTN13 appears relatively slow in comparison to non-membrane-shaping ER membrane proteins, as observed previously (5, 7) (Supplemental Fig. 2). In comparison, our previously described mutant ΔTM4, where the 4 TMDs of RTN13 were each shortened to a length of 17 residues (5) shows markedly higher mobility (Supplemental Fig. 2B and (4)), with a FRAP profile which is significantly different to that observed in full length RTN13 (Chi-squared test for trend; p-value 0.001; Supplemental Fig. 2E). In contrast, both the YFP-RTN13 mutant lacking the C-terminal region (Δ160-206; Supplemental Fig. 2C), and the I165K mutant (Supplemental Fig. 2D), displayed recovery kinetics that are comparable with those of full length (p-value 0.181 and 0.245, respectively). These data indicate that mutations affecting the putative APH regions do not affect the protein's capacity to form homo-oligomers.

We also used FRET-FLIM analysis to test whether the above mutants were still able to interact with full length RTN13. YFP (donor) was fused to the mutant RTN13 proteins and mCherry (mCh; acceptor) to the full length RTN13 sequence. Donor and acceptor constructs were co-infiltrated into *N. benthamiana* epidermal cells and FRET-FLIM used to assess protein-protein interactions. The lifetime values for each RTN13 pair is shown in Table 1. Supplemental Fig. 3 shows fluorescence lifetimes of 35S:YFP:RTN13 expressed alone or in combination with 35S:mCh:RTN13, as representative examples of the results obtained from FRET-FLIM analyses.

FRET-FLIM has been used extensively *in planta* to confirm protein-protein interactions identified through a range of other techniques (6, 15). A reduction in the lifetime of

donor fluorescence by as little as 0.2 ns in the presence of an acceptor fluorophore has been shown to be indicative of a direct interaction between two proteins such that they are in close enough proximity (1-10nm) for quenching to occur (15-17). Here, all of the combinations tested displayed at least a 0.35 ns decrease in lifetime when expressed as a donor/acceptor pair compared with expression of the donor alone (Table 1; Supplemental Fig. 3). Hence, removal of the APH or disruption of its hydrophobic face does not affect the ability of the protein to homo-oligomerise or to interact with the full length RTN13 isoform. This observation is in agreement with previous studies of RTN13 and other RTN interactions, where a truncated version of RTN13 lacking the two C-terminal TMDs was still shown to form homotypic interactions (6).

While the role of APHs in sculpting membranes has been well documented for several classes of proteins including Sar1, epsin, endophilin and ArfGAP1 ((18, 19) and references therein), the apparent absence of an APH in proteins of the RTN family suggested that their membrane-sculpting action arose from a combination of wedging, due to their membrane topology, and scaffolding, resulting from their ability to form immobile oligomers (7, 20). Indeed, altering the length of the TMD, both by shortening and extension, resulted in a loss of function. Altering TMD length, however, also impacted on the ability of the protein to oligomerise, making it impossible to assess the relative contribution of the two mechanisms described above. Our data indicate that the newly identified, conserved APH at the C terminus of RTN13 is necessary for its ability to shape ER tubules *in vivo*. Loss of the APH or mutations that disrupt its amphipathic nature do not affect RTN13's ability to form oligomers but abolish its capacity to constrict ER tubules. Previously, Shibata et al. (7) showed that mutants of ScRTN1p with defects in oligomerization were still able to induce ER tubule formation. In the light of the results presented here, we now suggest that this is likely due to the C-terminal APH region remaining unaffected in those mutants. In conclusion, while it is likely that the RHD alone is sufficient to guarantee reticulon oligomerisation, its main role may be to provide an environment for the correct insertion and interaction of the crucial membrane-shaping APH.

Materials and Methods

***In silico* analysis of RTN13.** A consensus prediction of the membrane topology of AtRTN13 was performed using TOPCONS (21) with further refinement of the position of

the TMDs based on sequence alignments with the human RTNs and experimental evidence described previously (5, 11). The predicted topology of RTN13 was plotted using the T_EXtopo package in LaTeX (22). Based on the alignment, a putative 16 amino acid APH in the region C-terminal to the TMD was identified in AtRTN13 using the HELIQUEST web server algorithm (23). The membrane-seeking properties of the AtRTN13 APH and the corresponding region in 250 sequences obtained from a BLAST search against the full AtRTN13 sequence were evaluated as described by Eisenberg *et al*. (24).

Generation of RTN13 constructs. A complete list of all primers used in this study is given in Supplemental Table 1. All PCRs were performed using high fidelity DNA polymerase (Accuzyme, Bioline). The coding region of RTN13 was cloned and fused to eYFP as previously described (4), and used to generate a YFP:RTN13 Gateway® Entry clone in pDONRZeo (ThermoFisher Scientific). A point mutation in the entry clone (I165K) was created through site directed mutagenesis PCR with overlapping forward and reverse primers containing the appropriate sequence mismatch, followed by digestion of the methylated template with 10 U *DpnI* (New England Biolabs) for 1 h at 37°C, and transformation into DH5α chemically competent *E. coli* cells. A mutated version of RTN13 in which the APH alone was excised (ΔAPH) was similarly created using overlapping primers homologous to the sequence before and after the desired deletion, in a two step process (deletion of E160-L169, followed by deletion of G170-K175). The native or mutated YFP:RTN13 in pDONRZeo was subsequently used as a PCR template to create an amplicon with *XbaI* and *SacI* recognition sites, which were then digested (*XbaI* and *SacI*, New England Biolabs), gel purified (QIAquick Gel Extraction kit, Qiagen) and ligated (T4 DNA ligase, ThermoFisher Scientific) into the corresponding sites in pVKH18-EN6 expression vector (25). A C-terminal truncation of RTN13 in which a stop codon was inserted after E159 (RTN13Δ160-206) was similarly generated. For FRET-FLIM analysis, a mCherry:RTN13 fusion was created by fusion PCR in which PCR fragments (10-50ng each) of mCherry with a 3' overhang to RTN13, and RTN13 with a 5' overhang to mCherry, were mixed and PCR amplified.

Transient expression analysis. All RTN13 constructs were transformed by heat-shock into *Agrobacterium tumefaciens* strain GV3101 and were transiently expressed in *Nicotiana benthamiana* leaf epidermal cells by agroinfiltration at an OD_{600} of 0.5, as previously described (26). In addition, serial dilutions of *Agrobacterium tumefaciens*

carrying the 35S:YFP:RTN13 construct were made from OD_{600} 0.5-0.05 for agroinfiltration.

Protein resolution and detection

Total proteins were isolated from infiltrated *N. benthamiana* leaves by homogenizing in a protein extraction buffer (0.2M NaCl, 1mM EDTA, 2% 2-mercaptoethanol, 0.2% Triton X-100, 0.1M Tris-HCl pH 7.8, complete protease inhibitor cocktail tablet [Roche Diagnostics Ltd]). For sucrose gradient analysis, ER microsomes were isolated from infiltrated leaves as described (27). Microsomal pellets were resuspended in 100µl TKMG lysis buffer (50 mM Tris-HCl, pH 7.0, 150 mM KCl, 2 mM $MgCl_2$, 10% glycerol, 1 mM EDTA, 1 mM PMSF, 1 mM 4-(2-aminoethyl)benzenesulfonylfluoride hydrochloride) containing 1% digitonin. Solubilized lysate was centrifuged for 10 min at 12,000 g to separate out any remaining leaf debris. Microsomes were loaded onto continuous 5-30% (w/v) sucrose gradients and ultracentrifuged at 166,000 g for 4h 30' at 25^{o}C in a Beckman SW55Ti rotor. Twenty gradient fractions were collected and subjected to SDS-PAGE on 15% acrylamide gels. 500 µg each of ferritin (440 kDa), aldolase (158 kDa) and ovalbumin (44 kDa) (GE Healthcare) were used as molecular weight standards, and stained with Coomassie Brilliant Blue R-250 following electrophoresis. Proteins were transferred onto PVDF membranes and subjected to immunoblotting with anti-GFP-HRP antisera (Miltenyi Biotec Ltd.). Immunoblots were developed by enhanced chemiluminescence (ECL; Promega) using a ImageQuant LAS4000 imaging system (GE Healthcare).

Confocal microscopy. Freshly excised leaf samples were mounted in water and imaged on a Leica TCS SP5 confocal microscope with a 63x oil immersion objective lens. GFP and eYFP were excited at 488 nm and 514 nm, respectively. GFP was detected in the 494-513 nm range and eYFP in the 524-554 range. Simultaneous detection of GFP and YFP was performed by combining the settings indicated above using the sequential scanning facility of the microscope, as instructed by the manufacturer. For FRAP analysis, samples were imaged with a Zeiss LSM880 equipped with a 63x oil immersion objective. YFP was excited at 514 nm and detected in the 520 to 560 nm range. For ER network analysis, samples were imaged using a 100X/1.46 NA oil immersion objective on a Zeiss LSM880 equipped with an Airyscan detector. Images were acquired using a defined region of interest with an average of 4 with 2048x2048 pixels of image size and 8 bit image depth, taking care that every part of each image remained fully within the dynamic range of pixel intensity.

Colocalisation analysis. Colocalisation analysis was completed using the ImageJ-based open source processing package Fiji v1.49r (28). First a median filter (radius=0.5 pixels) was used to reduce salt and pepper noise and a rolling ball filter (radius=20 pixels) was used to reduce the background noise in each image. The RGB image was then split into 8-bit red and green channel images, and an ROI for each image was selected. Saturation level was set at 0.1% to normalise the images. Minimum pixel intensity was set to 0 for each channel. To measure the Pearson's Coefficient the CoLoc_2 plugin was used (point spread function=3px and Costes iterations=50). A minimum of 8 images, corresponding to 8 different cells, was used for each RTN construct.

ER network analysis. ER cisternae were automatically segmented from single plane (*x,y*) images collected with the AiryScan detector by an image opening step to remove all features smaller than maximum tubule diameter (estimated as the full-width half-maximum (FWHM) from a manual transect). This was followed by an active-contour step to shrink the segmented region back to match the intensity profile of the cisternae. To automatically extract the tubular ER network, images were background subtracted then rescaled using contrast-limited adaptive histogram equalisation (CLAHE). The ER tubules were enhanced using a series of oriented log Gabor filters, typically applied over 5 spatial scales and six orientations to calculate the local phase-congruency (29-31). Whilst the phase-congruency filters characterise a number of relevant image properties, the local weighted mean phase angle ('Feature type') provided the most robust subsequent segmentation. The tubular network was segmented from the feature type image using hysteresis thresholding and binary thinning to give a single-pixel wide skeleton. To ensure closely appressed regions were not merged during the hysteresis threshold, all local intensity minima were identified using an h-minimum transform and set to zero.

The width of the tubules was estimated by several different methods. To estimate the tubule FWHM, the peak height was estimated from the intensity, sampled for each pixel in the skeleton; the distance was estimated from the distance transform of the pixel skeleton; and the 50% threshold estimated from where the pixel intensity falls below half the peak, assuming a local background of zero after background subtraction. This returns the FWHM of the object convolved with the point-spread function. Alternatively, a granulometry approach was used whereby the intensity image was subjected to a series of image openings (erosion followed by dilation) that successively removed structures as the size of the opening kernel exceeds the underlying object. This results in

an intermediate (*x,y,s*) image, where *s* increases with the size of the disk-shaped kernel. The intensity of each pixel initially decreases slowly with *s* as the kernel samples more of the object, but then reduces dramatically once the boundary of the object is reached, and the kernel only samples the background. The transition point for any pixel is determined from the maximum (negative) gradient of the granulometry curve. However, this approach constrains the radius to integer pixels values, and also suffers from digital approximation of small kernels to a true disk shaped kernel. Thus, rather than extract a specific size threshold, the integrated intensity under the granulometry curve was calculated to provide a more nuanced interrogation of the local image intensity profile. The integrated intensity cannot be directly related to the physical width without additional assumptions about the relationship between fluorescence intensity and sampled volume. Nevertheless, this approach does help with estimation of relative tubule widths, even if they are sub-resolution objects, provided it is assumed that the fluorescent probe is evenly distributed throughout the ER, and the ER is within the sampling volume of the confocal defined by the point-spread-function (psf). The average intensity from the cisternal regions was taken as a measure of a fully-filled psf would yield when sampling sheets and tubes, and used to normalise the integrated intensity values between images.

The pixel skeleton was converted to a graph representation with nodes at the junctions, cisternae and free ends, connected by edges along each tubule. Bulges along each tubule were estimated from peaks in the integrated intensity profile that were at least 10% of the maximum intensity and also 5% greater than the signal on either side. Likewise, constrictions were determined using the same peak-finding process on the inverted intensity profile.

All the analysis routines were implemented in MATLAB (The Mathworks, Nantick, MA) and are available in a standalone package or a MATLAB app from www.markfricker.org.

FRAP analysis. For photobleaching, the tubular ER was magnified using a 10× zoom for clear tubule detection. No drugs were used and stationary regions of the network were targeted for bleaching. Images were acquired every 0.41 s. Three prebleaching frames were acquired and a region of interest 5 μm in diameter bleached at 100% laser intensity for 1 frame. After photobleaching, 46 frames were taken at 0.41 s intervals for a total of 21 s. Mean fluorescence intensity within the bleached area was measured during the recovery phase of FRAP experiments using Zeiss ZEN software. Analysis of fluorescence recovery was performed as described by Shibata *et al.* (2008). Briefly, the fluorescence intensity of three regions of interest was measured: the photobleached

region (PR), a region outside of the tubular ER network providing overall background fluorescence (BR), and a region within the ER network that was not photobleached to correct for overall observational photobleaching and fluorescence variation (CR). The relative fluorescence intensity (I) for each individual FRAP experiment was background corrected and normalised using the following equation:

$I=[(PR_t - BR_t)/(PR_{t0} - BR_{t0})*100]x[(100-CR_t/CR_{t0})/100]+1$

where t_0 values were averaged over the three pre-bleach scans. Normalised data for each set of FRAP experiments were plotted and a Chi-square test for trend performed using GraphPad Prism 6.0 to compare the recovery curves of each mutant to that of wild-type.

FRET-FLIM analysis. Data acquisition for FRET-FLIM was performed as described by Sparkes et al. (2010). Data were analyzed by obtaining excited state lifetime values of a region of interest on the nucleus, and calculations were made using the SPCImage 5.4 analysis software (Becker and Hickl). The distribution of lifetime values within the ROI were generated and displayed as a curve. Only values that had a Chi-squared score between 0.9 and 1.4 were used. The median lifetime value and minimum and maximum values for a quarter of the median lifetime values from the curve were taken to generate the range of lifetimes per sample. At least three nuclei per RTN combination were analyzed, and the average of the ranges taken. Results are from two independent experiments.

Peptide Synthesis and Purification. A peptide corresponding to RTN13 residues 160-175 (EYGDQIQKHLGSLKDK) was synthesized at Insight Biotechnology Limited (Wembley, UK) using F-moc chemistry. The peptide was purified by reversed-phase high performance liquid chromatography (HPLC) using a linear acetonitrile gradient from 30-100% containing 0.1% trifluoroacetic acid (TFA) on a Phenomenex C4 semi-preparative column. The purity of pooled peptide fractions was confirmed by electrospray ionization time-of-flight mass spectroscopy (ESI-TOF-MS microTOF, Bruker) before subsequent lyophilization.

Circular Dichroism (CD). CD spectra were measured using a Jasco J-1500 spectropolarimeter equipped with a Peltier thermally controlled cuvette holder (Jasco UK, Great Dunmow, UK) and 1.0 mm path-length quartz cuvettes (Starna, Optiglass Ltd, Hainault, UK). All spectra were recorded from 190 to 300 nm using a 2.0 nm spectral bandwidth, 0.1 nm step resolution, 100 nm min^{-1} scanning speed, and 1 s response time.

The peptide was prepared in 25 mM sodium phosphate buffer (pH 7.0) in the presence and absence of the zwitterionic detergent n-dodecylphosphocholine (DPC, Avanti Polar Lipids, USA) at increasing concentrations ranging from 10-200 mM, maintaining a constant peptide concentration of 94 μM. CD spectra shown were collected at 37°C, and were averaged from four individual spectra after subtraction of the CD spectrum of the buffer or buffer/detergent solution (as appropriate). CD data were fitted using Dichoweb (Contin/training set 7) (32-34) to estimate the secondary structure content.

Acknowledgements

This work was funded by the BBSRC ERA-CAPS grant 'PER ASPERA' to LF and CH. We are grateful to the BBSRC for a DTP studentship to ND. We thank Philip Young for help with FRAP analysis.

Author contributions

EB generated the constructs, performed the majority of the experiments and co-wrote the manuscript; ND performed colocalization analysis; VK performed Airyscan image acquisition; RB and AD performed CD analysis; SB assisted in the production of FRET-FLIM data; JB and JS carried out sequence alignments and APH predictions; CH helped with data analysis and manuscript preparation; MDF developed the ER analysis tool and performed the analysis. LF conceived the study, performed some of the FRET-FLIM experiments and co-wrote the manuscript.

References

1. Hawes C, Kiviniemi P, Kriechbaumer V (2015) The endoplasmic reticulum: A dynamic and well-connected organelle. *J Integr Plant Biol* 57(1):50–62.

2. Zhang M, et al. (2013) ROOT HAIR DEFECTIVE3 family of dynamin-like GTPases mediates homotypic endoplasmic reticulum fusion and is essential for Arabidopsis development. *PLANT PHYSIOLOGY* 163(2):713–720.

3. Chen J, Stefano G, Brandizzi F, Zheng H (2011) Arabidopsis RHD3 mediates the generation of the tubular ER network and is required for Golgi distribution and motility in plant cells. *Journal of Cell Science* 124(Pt 13):2241–2252.

4. Tolley N, et al. (2008) Overexpression of a Plant Reticulon Remodels the Lumen of the Cortical Endoplasmic Reticulum but Does not Perturb Protein Transport. *Traffic* 9(1):94–102.

5. Tolley N, et al. (2010) Transmembrane domain length is responsible for the

ability of a plant reticulon to shape endoplasmic reticulum tubules in vivo. *Plant J* 64(3):411–418.

6. Sparkes I, et al. (2010) Five Arabidopsis reticulon isoforms share endoplasmic reticulum location, topology, and membrane-shaping properties. *Plant Cell* 22(4):1333–1343.

7. Shibata Y, et al. (2008) The reticulon and DP1/Yop1p proteins form immobile oligomers in the tubular endoplasmic reticulum. *Journal of Biological Chemistry* 283(27):18892–18904.

8. Voeltz GK, Prinz WA, Shibata Y, Rist JM, Rapoport TA (2006) A class of membrane proteins shaping the tubular endoplasmic reticulum. *Cell* 124(3):573–586.

9. Hu J, et al. (2008) Membrane proteins of the endoplasmic reticulum induce high-curvature tubules. *Science* 319(5867):1247–1250.

10. Zurek N, Sparks L, Voeltz G (2011) Reticulon short hairpin transmembrane domains are used to shape ER tubules. *Traffic* 12(1):28–41.

11. Brady JP, Claridge JK, Smith PG, Schnell JR (2015) A conserved amphipathic helix is required for membrane tubule formation by Yop1p. *Proc Natl Acad Sci USA*:201415882.

12. Liu TY, Bian X, Sun S, Hu X (2012) Lipid interaction of the C terminus and association of the transmembrane segments facilitate atlastin-mediated homotypic endoplasmic reticulum fusion doi:10.1073/pnas.1208385109/-/DCSupplemental/pnas.201208385SI.pdf.

13. Faust JE, et al. (2015) The Atlastin C-terminal Tail is an Amphipathic Helix that Perturbs Bilayer Structure during Endoplasmic Reticulum Homotypic Fusion. *J Biol Chem* 290(8):1–13.

14. Eisenberg D, Schwarz E, Komaromy M, Wall R (1984) Analysis of membrane and surface protein sequences with the hydrophobic moment plot. *Journal of Molecular Biology* 179(1):125–142.

15. Kriechbaumer V, et al. (2015) Reticulomics: Protein-Protein Interaction Studies with Two Plasmodesmata-Localized Reticulon Family Proteins Identify Binding Partners Enriched at Plasmodesmata, Endoplasmic Reticulum, and the Plasma Membrane. *PLANT PHYSIOLOGY* 169(3):1933–1945.

16. Stubbs CD, Botchway SW, Slater SJ, Parker AW (2005) The use of time-resolved fluorescence imaging in the study of protein kinase C localisation in cells. *BMC Cell Biol* 6(1):22.

17. Osterrieder A, et al. (2009) Fluorescence Lifetime Imaging of Interactions between Golgi Tethering Factors and Small GTPases in Plants. *Traffic* 10(8):1034–1046.

18. Shen H, Pirruccello M, Pietro De Camilli (2012) SnapShot: Membrane Curvature Sensors and Generators. *Cell* 150(6):1300–1300.e2.

19. Suetsugu S, Kurisu S, Takenawa T (2014) Dynamic Shaping of Cellular Membranes by Phospholipids and Membrane-Deforming Proteins. *Physiological*

Reviews 94(4):1219–1248.

20. Zimmerberg J, Kozlov MM (2005) How proteins produce cellular membrane curvature. *Nat Rev Mol Cell Biol* 7(1):9–19.

21. Tsirigos KD, Peters C, Shu N, Käll L, Elofsson A (2015) The TOPCONS web server for consensus prediction of membrane protein topology and signal peptides. *Nucleic Acids Research* 43(W1):W401–7.

22. Beitz E (2000) TEXtopo: shaded membrane protein topology plots in LaTEX2ε. *Bioinformatics* 16(11):1050–1051.

23. Gautier R, Douguet D, Antonny B, Drin G (2008) HELIQUEST: a web server to screen sequences with specific alpha-helical properties. *Bioinformatics* 24(18):2101–2102.

24. Eisenberg D, Weiss RM, Terwilliger TC (1982) The helical hydrophobic moment: a measure of the amphiphilicity of a helix. *Nature* 299(5881):371–374.

25. Batoko H, Zheng HQ, Hawes C, Moore I (2000) A rab1 GTPase is required for transport between the endoplasmic reticulum and golgi apparatus and for normal golgi movement in plants. *THE PLANT CELL ONLINE* 12(11):2201–2218.

26. Sparkes IA, Runions J, Kearns A, Hawes C (2006) Rapid, transient expression of fluorescent fusion proteins in tobacco plants and generation of stably transformed plants. *Nat Protoc* 1(4):2019–2025.

27. Aggarwal C, et al. (2014) Blue-light-activated phototropin2 trafficking from the cytoplasm to Golgi/post-Golgi vesicles. *Journal of Experimental Botany* 65(12):3263–3276.

28. Schindelin J, et al. (2012) Fiji: an open-source platform for biological-image analysis. *Nat Meth* 9(7):676–682.

29. Kovesi PD (1999) *Image Feature from Phase Congruency, Videre: Journal of Computer Vision Research*. 1(3)

30. Obara B, Grau V, Fricker MD (2012) A bioimage informatics approach to automatically extract complex fungal networks. *Bioinformatics* 28(18):2374–2381.

31. Kovesi PD (2000) MATLAB and Octave functions for computer vision and image processing. Available from http://www.peterkovesi.com/matlabfns/

32. Whitmore L, Wallace BA (2004) DICHROWEB, an online server for protein secondary structure analyses from circular dichroism spectroscopic data. *Nucleic Acids Research* 32(Web Server issue):W668–73.

33. Whitmore L, Wallace BA (2008) Protein secondary structure analyses from circular dichroism spectroscopy: Methods and reference databases. *Biopolymers* 89(5):392–400.

34. Sreerama N, Woody RW (2000) Estimation of Protein Secondary Structure from Circular Dichroism Spectra: Comparison of CONTIN, SELCON, and CDSSTR Methods with an Expanded Reference Set. *Analytical Biochemistry* 287(2):252–

260.

Figure Legends

Figure 1. RTN13 possesses a putative, conserved C-terminal APH. (A) Schematic topology model of RTN13 in the ER membrane (total length, 206 amino acids). The positions of the four TMDs of the RHD (predicted using the TOPCONS web server (21)) are indicated alongside the APH. Residues are coloured by hydropathy whereby red is acidic, blue is basic, yellow is polar uncharged, and green is hydrophobic/nonpolar. Selected amino acids referred to in the text are indicated **(B)** Protein sequence alignment of the RHD and C-terminal region of *Arabidopsis thaliana* RTN13, *Homo sapiens* RTN1-4 and *Saccharomyces cerevisiae* Yop1p. Residues are coloured as in (A) with the exception of polar uncharged amino acids, coloured orange. Numbering is for RTN13 amino acid positions **(C)** Helical wheel plot of the identified region of highest predicted hydrophobic moment of RTN13 C-terminal to the RHD and of the mutated form RTN13 I165K. The direction (line) and size (square) of the hydrophobic moment (μ) of the helices are depicted in pink (μ=0.28 [WT] and 0.18 [I165K]) **(D)** Plot of hydrophobic moment against hydrophobicity for the APH of RTN13 and the same region from 250 sequences obtained by a BLAST search against the full RTN13 sequence. The position of RTN13 is indicated (red star). The majority of the sequences lie in the region of the plot expected for membrane-seeking helices (24). **(E)** Schematic representation of the constructs used in this study (not to scale). TM, transmembrane domain; APH, putative amphipathic helix; CT, C-terminal region. KKSE, ER retention motif

Figure 2. RTN13 residues 160-175 form an α-helix in the presence of detergent micelles. CD spectra of the putative APH peptide (EYGDQIQKHLGSLKDK, residues 160-175) dissolved in 25 mM sodium phosphate buffer (pH 7.0, dashed line) as well as increasing concentrations of buffer-solubilized micelles. The peptide attained a maximum helical content of 31% in 200 mM DPC (as estimated by fitting of the data as described in Materials and Methods). CD data fitting summary: Helix: 30.6%, Strand: 21.3%, Turns: 19.6%, disordered: 27.8%

Figure 3. Deletion of the APH or disruption of its hydrophobic face impairs RTN13 function. *Nicotiana benthamiana* epidermal cells were co-infiltrated with *Agrobacterium tumefaciens* carrying plasmids encoding either full length, mutant or truncated forms of 35S:YFP:RTN13, together with the soluble ER marker, GFP-HDEL. Representative confocal images of leaves transfected with **(A)** 35S:YFP:RTN13 **(B)** 35S:YFP:RTN13Δ160-206 **(C)** 35S:YFP:RTN13 I165K **(D)** 35S:YFP:RTN13 ΔAPH. Scale bar = 5μm. **(E)** Average Pearson's correlation coefficients (PCCs) of cells coexpressing GFP-HDEL and full length, truncated or mutated forms of 35S:YFP:RTN13, where a PCC of +1 indicates perfect colocalisation, 0 indicates no colocalisation and -1 indicates negative colocalisation. Error bars indicate the standard error of the mean; n=8-9 cells. Asterisks indicate a significant difference between full length RTN13 and the relevant APH mutant (Student's t-test; $p<0.001$).

Figure 4. The APH is necessary for the action of RTN13 on the diameter of ER tubules.

(A) *Nicotiana benthamiana* epidermal cells were co-infiltrated with *Agrobacterium tumefaciens* carrying plasmids encoding the indicated constructs. Cells were imaged with a Zeiss Airyscan detector (left-hand panels) and subjected to ER network analysis (right-hand panels). **(B)** comparison of average ER tubule width and constrictions resulting from the expression of full length YFP-RTN13 or the APH mutants. Asterisks indicate significant differences (Student's t-test; $p<0.001$).

Figure 5. Removal or mutation of the APH does not affect the capacity of the resulting RTN13 protein to form oligomers within the ER membrane.

Microsomal membranes isolated from infiltrated *N. benthamiana* leaves expressing the indicated constructs were solubilized in 1% digitonin and separated on sucrose sedimentation velocity gradients. Gradient fractions were resolved by SDS-PAGE and gels subjected to immunoblotting with anti-GFP antiserum. Molecular weight markers (kDa) are indicated at the top and on the left. The immunoblot for Δ160-206 is overexposed due to the lower protein levels of this mutant (Supplemental Fig. 1A).

Table 1. Fluorescence lifetimes of RTN13 pairs in FRET-FLIM analysis. Full length (35S:mCh:RTN13; acceptor) and mutated or truncated forms of RTN13 (35S:YFP:RTN13Δ160-206 or I165K; donor) were infiltrated alone or in combination

into *N. benthamiana* leaf epidermal cells and protein-protein interactions assessed by FRET-FLIM analysis. For each measurement, a region of low mobility ER continuous with the nuclear envelope was selected and the fluorescence lifetime of the donor fluorophore measured. Table shows the range of FLIM lifetimes, mean and standard deviation (n=3-5 cells) and the p-values from Student's t-test comparisons of donor+acceptor compared to donor alone, which indicate that mutated and truncated forms of RTN13 are still able to oligomerise.

Supplemental Figure 1. **(A)** Protein expression of YFP-RTN13 and APH mutants. Equal amounts of protein from total protein extracts of agroinfiltrated *N. benthamiana* leaf sectors were subjected to SDS-PAGE and immunoblot with anti GFP antiserum. CBB, Coomassie brilliant blue staining of the post-ECL blot. Numbers at right indicate molecular weight marker in kD.
(B) As in A, but with extracts from leaves agroinfiltrated with the indicated OD_{600} of agrobacteria carrying plasmid encoding YFP-RTN13.
(C) *Nicotiana benthamiana* epidermal cells were co-infiltrated with the indicated OD_{600} of *Agrobacterium tumefaciens* carrying plasmids encoding full length 35S:YFP:RTN13 , together with the soluble ER marker, GFP-HDEL.

Supplemental Figure 2. *Nicotiana benthamiana* epidermal cells were infiltrated with *Agrobacterium tumefaciens* carrying plasmids encoding either full length, mutated or truncated forms of 35S:YFP:RTN13 and subjected to FRAP analysis. **(A-D)** Representative pre-bleaching and 0, 10 and 20 s frames from typical FRAP experiments. The circled areas represent regions undergoing photobleaching. Scale bar = 5μm **(A)** 35S:YFP:RTN13 **(B)** 35S:YFP:RTN13ΔTM4 **(C)** 35S:YFP:RTN13Δ160-206 **(D)** 35S:YFP:RTN13 I165K **(E)** Fluorescence intensities normalized to pre-bleaching values plotted over time. Error bars indicate the standard error; n=9-14 cells. The results of a Chi-squared test for trend (df=1) comparing the FRAP profile of each mutant to that of wild-type are shown (** $p<0.005$).

Supplemental Figure 3. FRET-FLIM analysis. Fluorescence lifetime data of 35S:YFP:RTN13 (donor) expressed alone or in combination with 35S:mCh:RTN13 (acceptor), as representative examples of the results obtained from FRET-FLIM analyses. (A) 35S:YFP:RTN13 alone (B) 35S:YFP:RTN13 + 35S:mCh:RTN13.
(i) A region of interest (ROI) on the ER continuous with the nuclear envelope was selected based on the lifetime decay curves of points within the region having a χ^2

value between 0.9 and 1.4 (iv). Pseudocoloured lifetime maps (ii) depict the lifetime of points within the ROI, and the distribution of lifetimes across the entire image is shown in (iii).

Supplemental Table 1. Oligonucleotide primers used for the generation of the RTN13 constructs in this study.

Figure 1

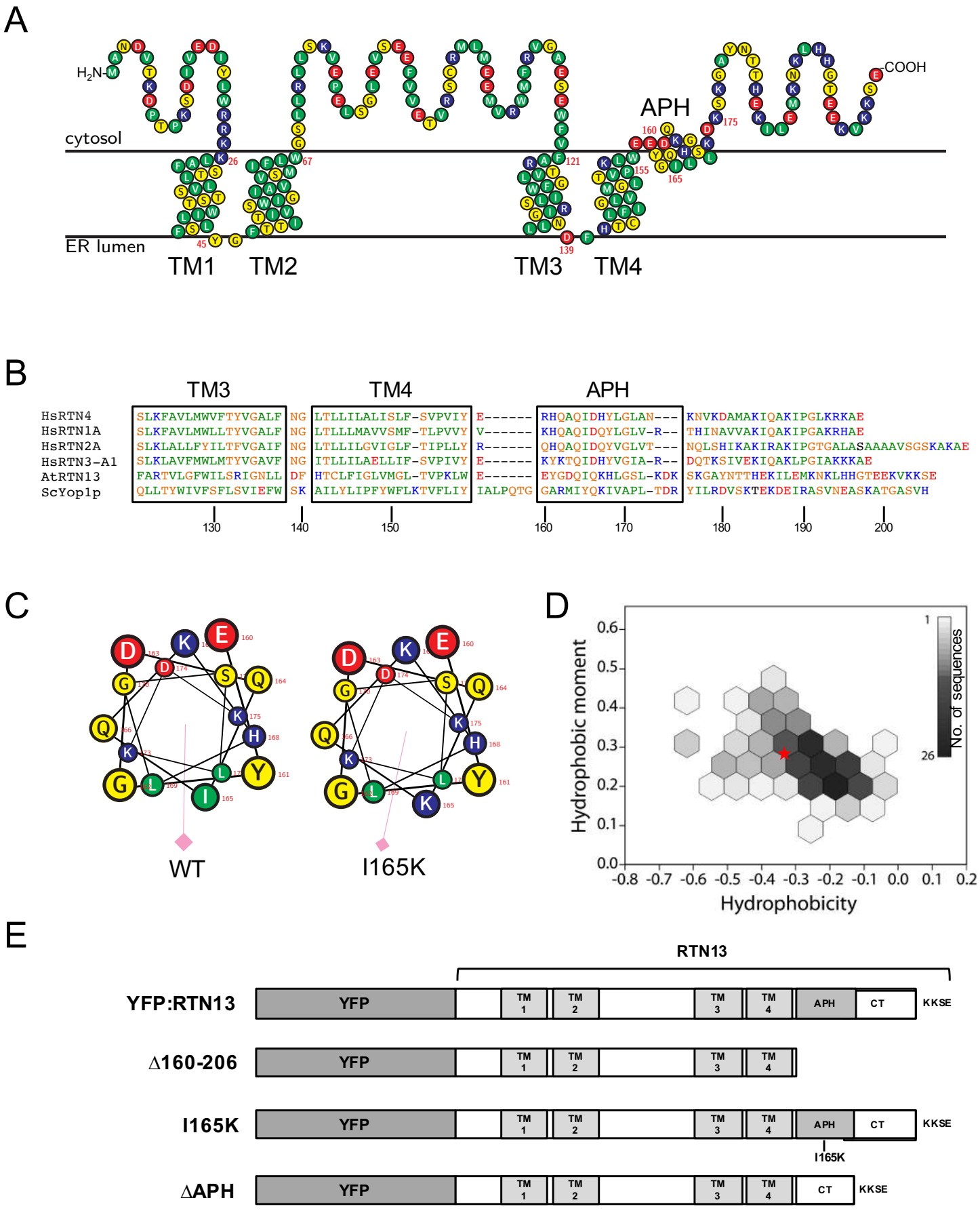
A
H2N-
-COOH
cytosol
ER lumen
APH
TM1
TM2
TM3
TM4
B
TM3
TM4
APH
HsRTN4
HsRTN1A
HsRTN2A
HsRTN3-A1
AtRTN13
ScYop1p
C
WT
I165K
D
Hydrophobic moment
Hydrophobicity
No. of sequences
E
RTN13
YFP:RTN13
Δ160-206
I165K
ΔAPH
YFP
TM 1
TM 2
TM 3
TM 4
APH
CT
KKSE

Figure 2

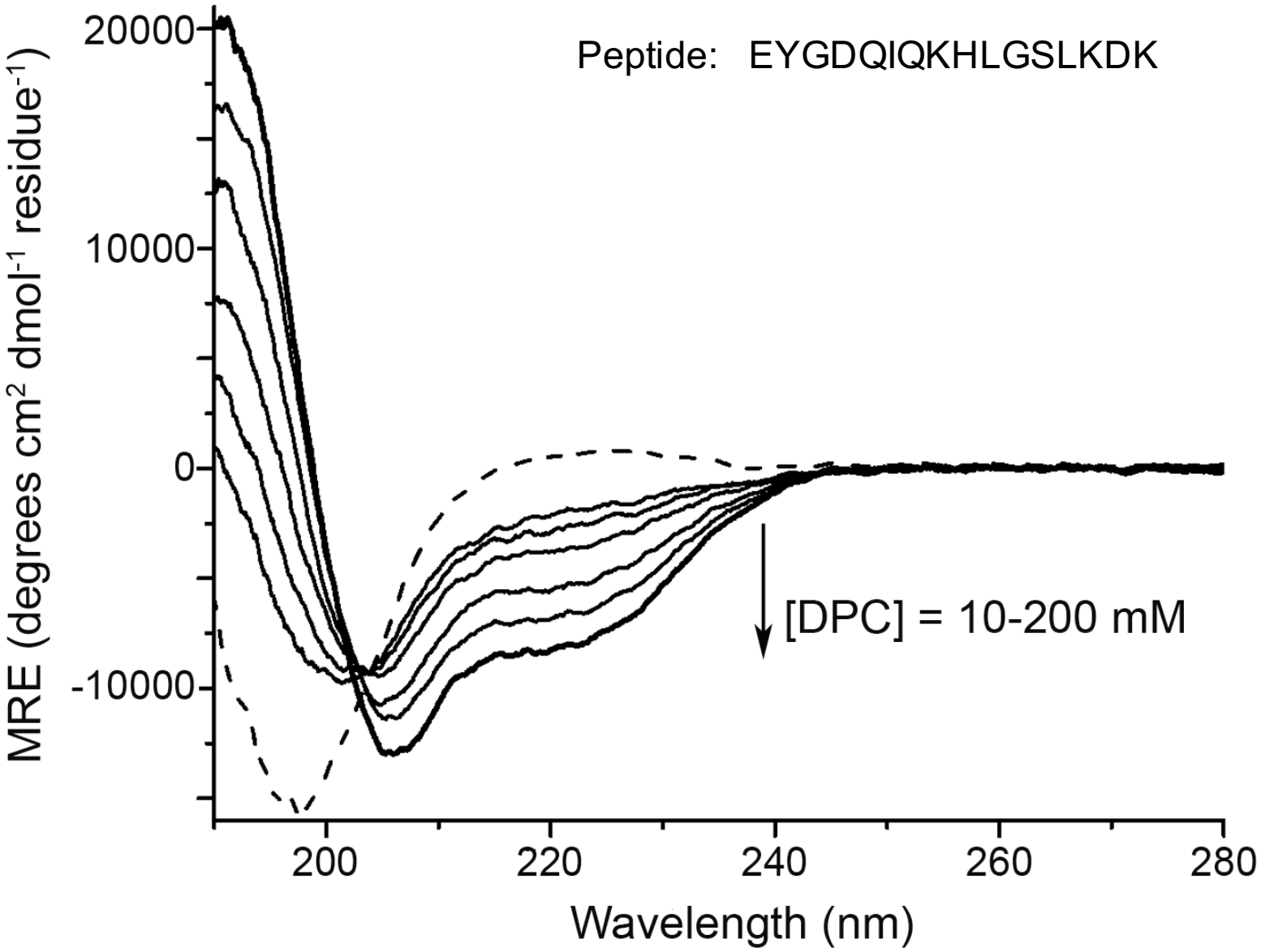
Peptide: EYGDQIQKHLGSLKDK
[DPC] = 10-200 mM
MRE (degrees cm2 dmol-1 residue-1)
20000
10000
0
-10000
200
220
240
260
280
Wavelength (nm)

Figure 3

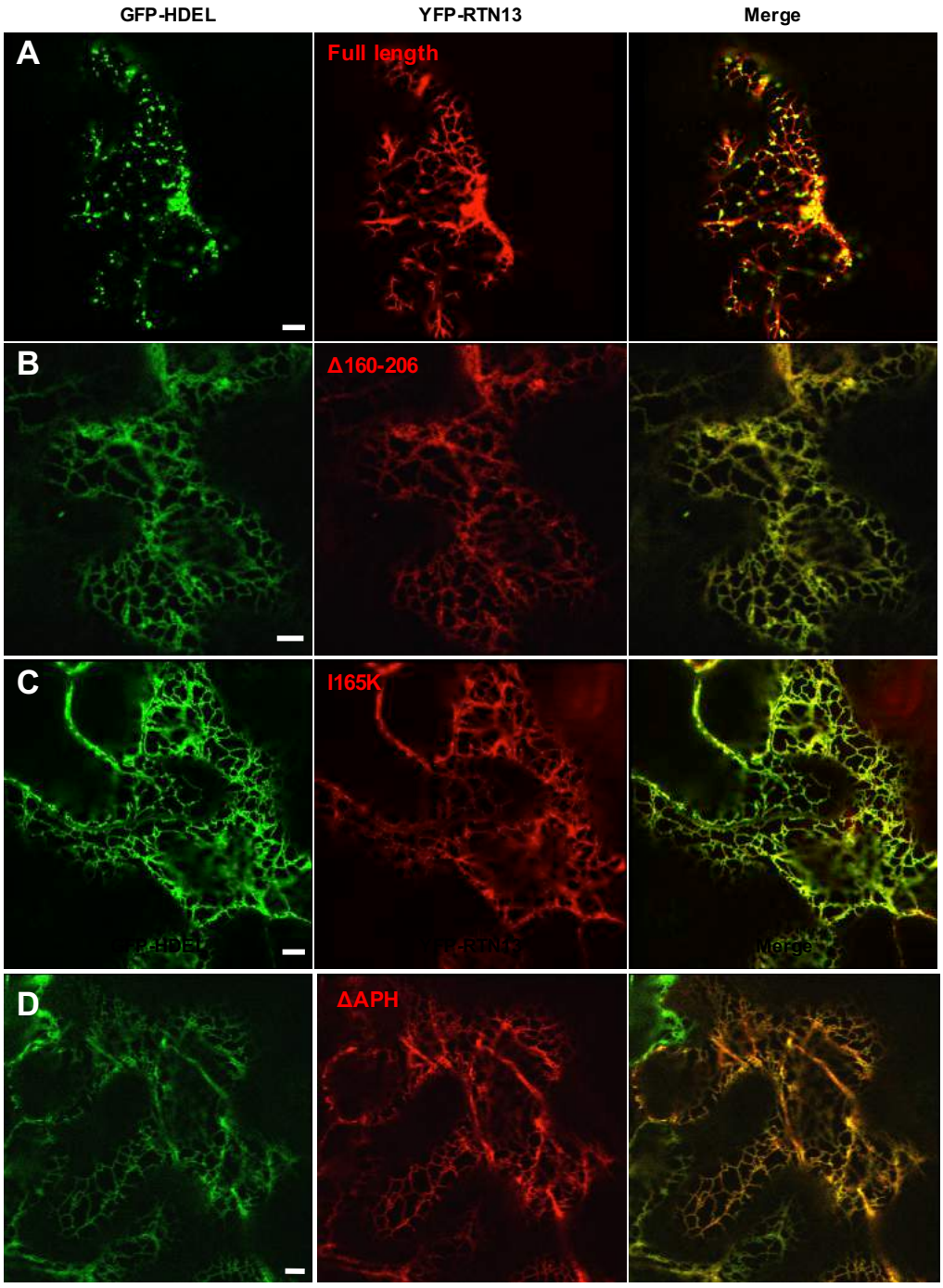
GFP-HDEL
YFP-RTN13
Merge
A
Full length
B
Δ160-206
C
I165K
D
ΔAPH

E

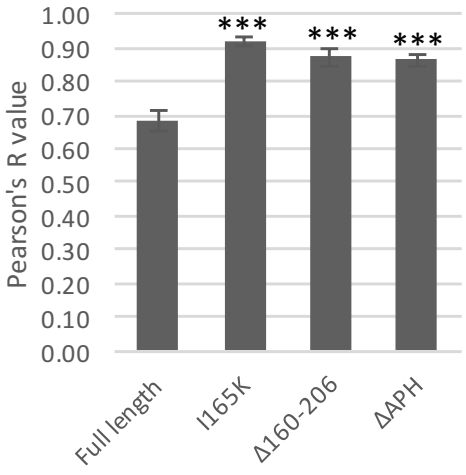
Pearson's R value
1.00
0.90
0.80
0.70
0.60
0.50
0.40
0.30
0.20
0.10
0.00
***
***
***
Full length
I165K
Δ160-206
ΔAPH

Figure 4

A

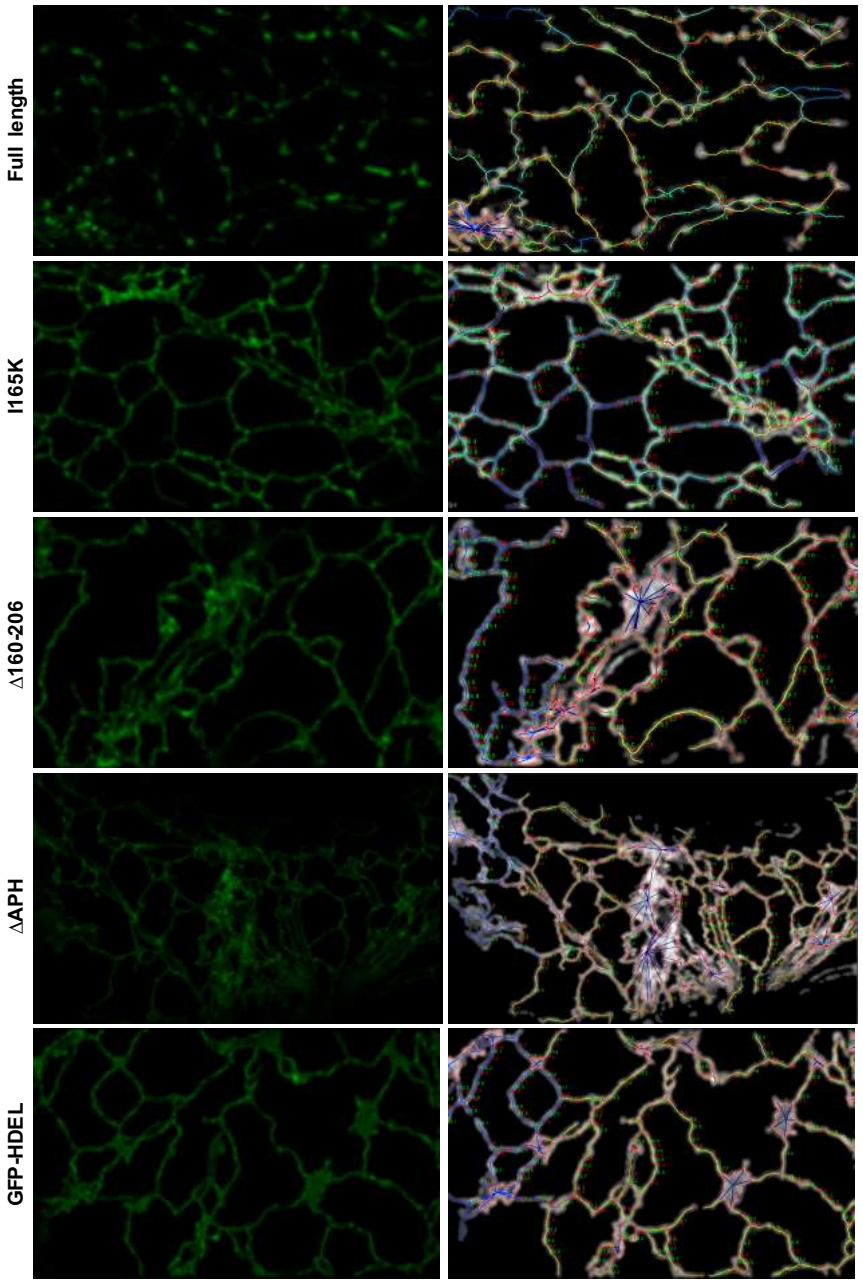
Full length
I165K
Δ160-206
ΔAPH
GFP-HDEL

B

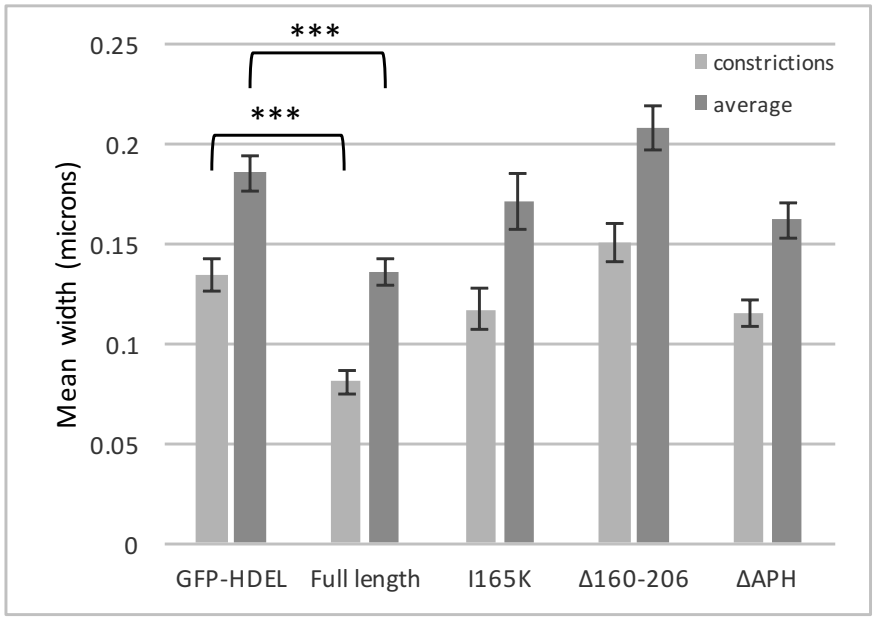
***
***
0.25
0.2
0.15
0.1
0.05
0
Mean width (microns)
constrictions
average
GFP-HDEL
Full length
I165K
Δ160-206
ΔAPH

Table 1

Donor	Acceptor	Range of FLIM Lifetimes (ns)	Mean FLIM Lifetime (ns)	Std Dev (ns)	P value (two-tailed Student's *t*-test)
YFP:RTN13	-	2.85-3.03	2.96	0.09	0.0002
YFP:RTN13	mCh:RTN13	2.42-2.61	2.50	0.07	
YFP:RTN13Δ160-206	-	3.0-3.1	3.03	0.06	0.0238
YFP:RTN13Δ160-206	mCh:RTN13	2.5-2.8	2.68	0.16	
YFP:RTN13 I165K	-	2.7-3.0	2.82	0.13	0.0049
YFP:RTN13 I165K	mCh:RTN13	2.40-2.56	2.46	0.07	

Figure 5

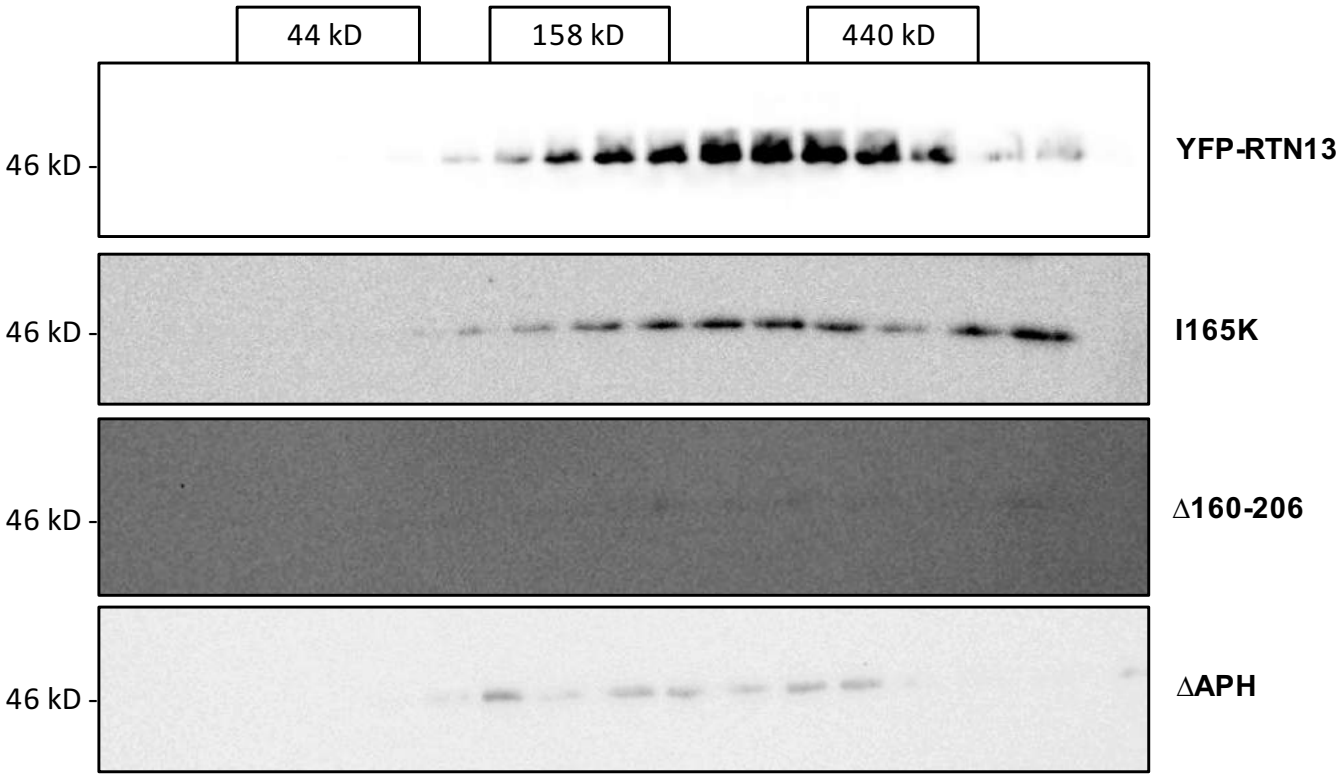
44 kD
158 kD
440 kD
46 kD
YFP-RTN13
46 kD
I165K
46 kD
Δ160-206
46 kD
ΔAPH

Supplemental Figure 1

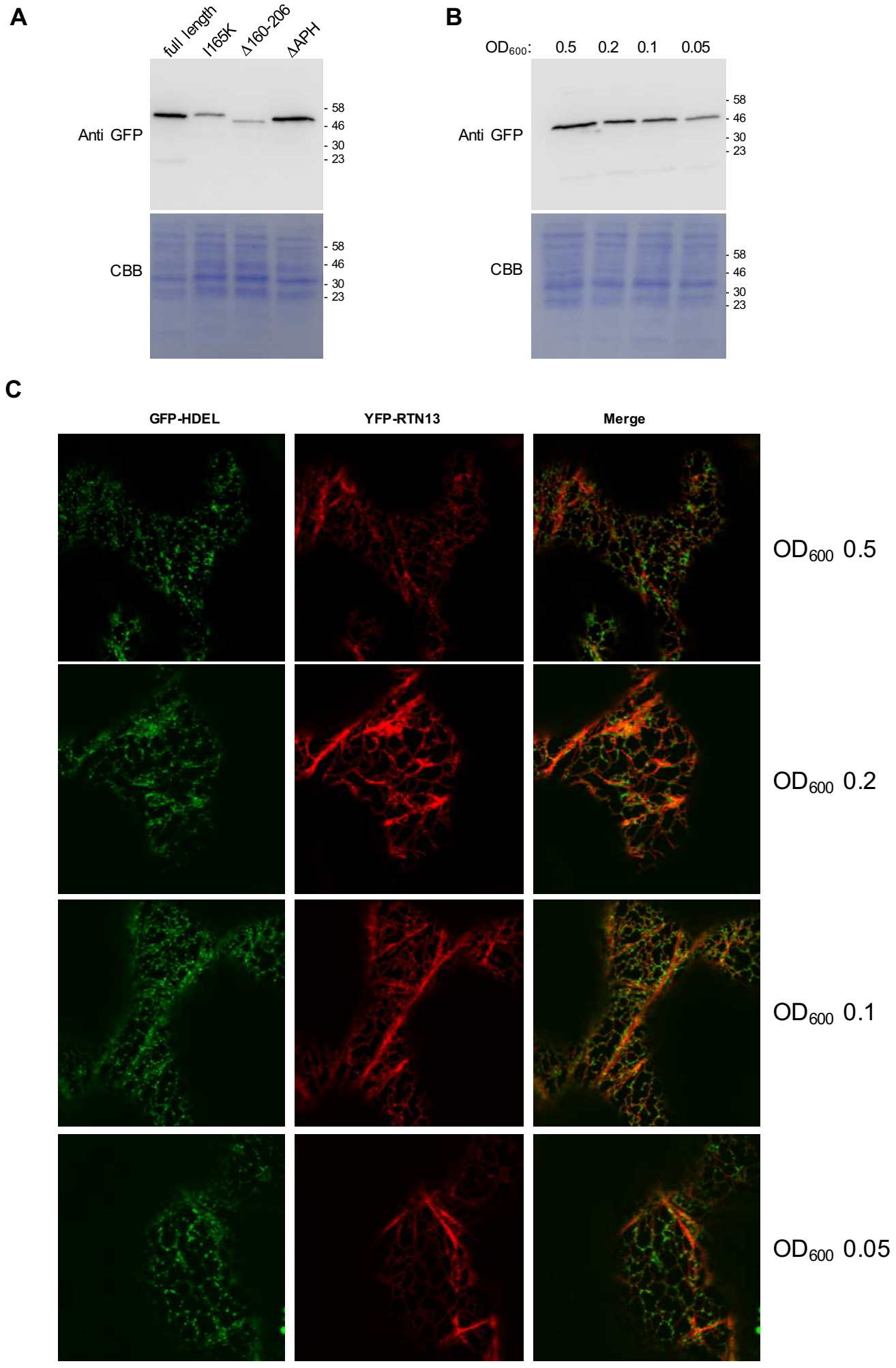

Supplemental Figure 2

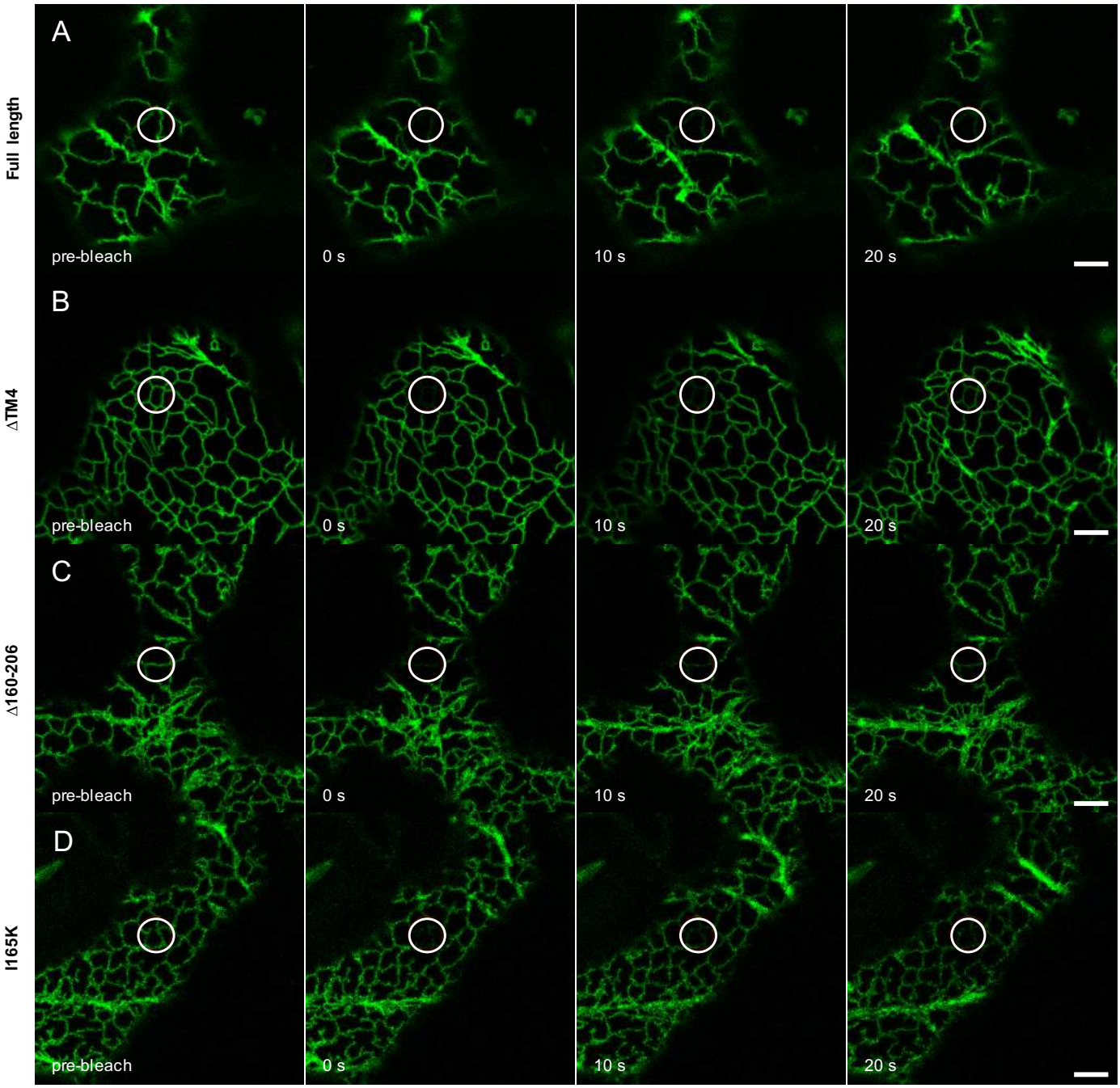

E

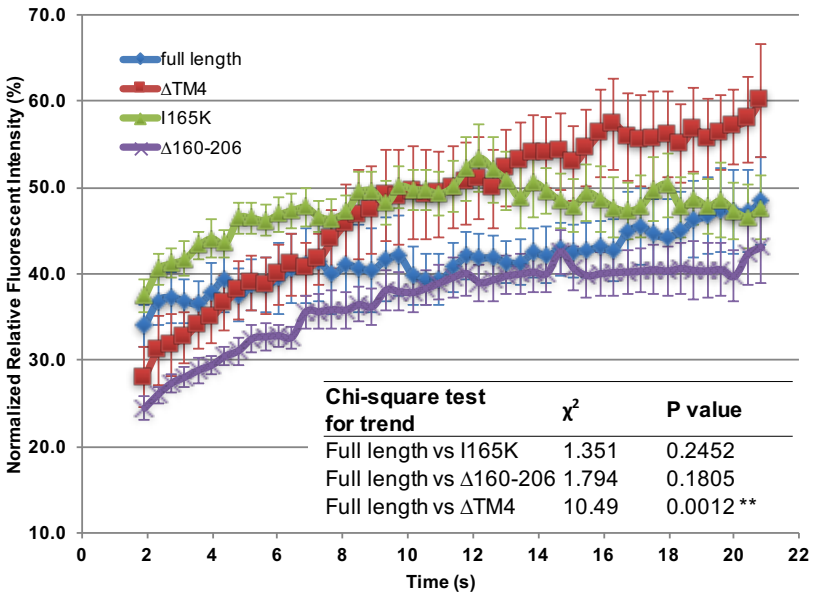

Chi-square test for trend	χ^2	P value
Full length vs I165K	1.351	0.2452
Full length vs Δ160-206	1.794	0.1805
Full length vs ΔTM4	10.49	0.0012 **

Supplemental Figure 3

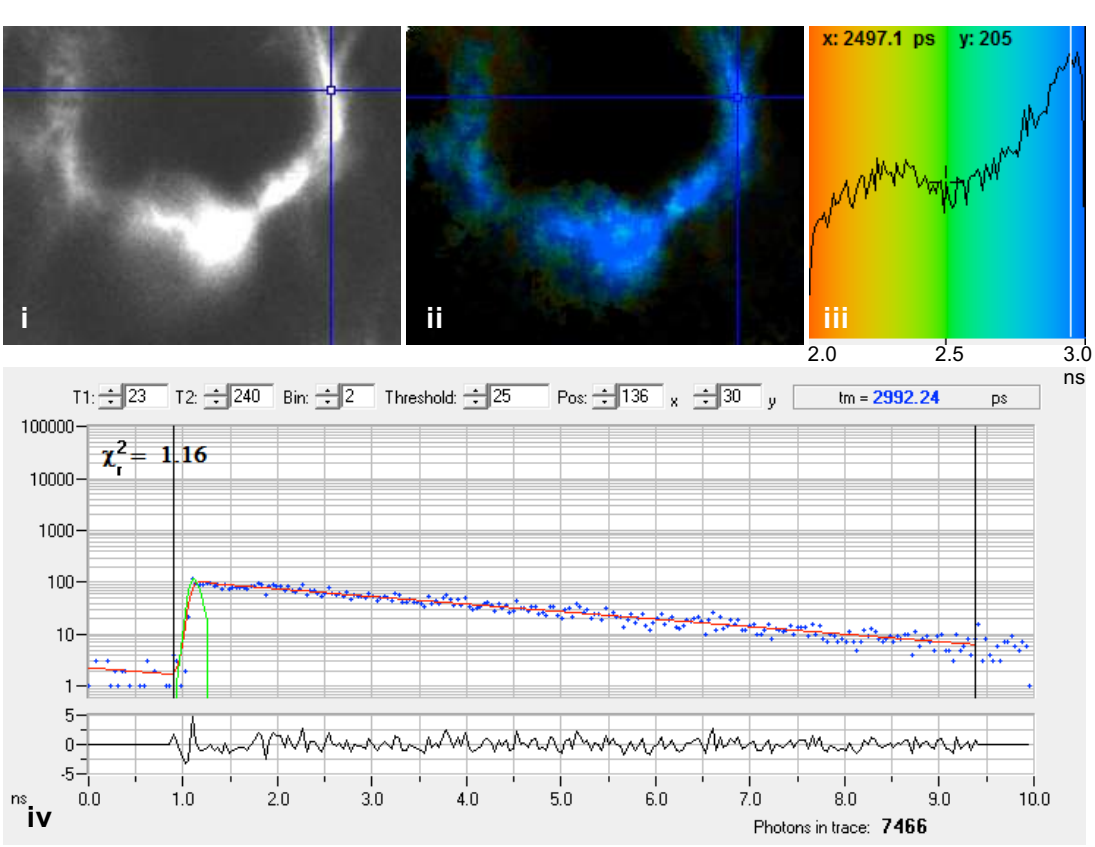

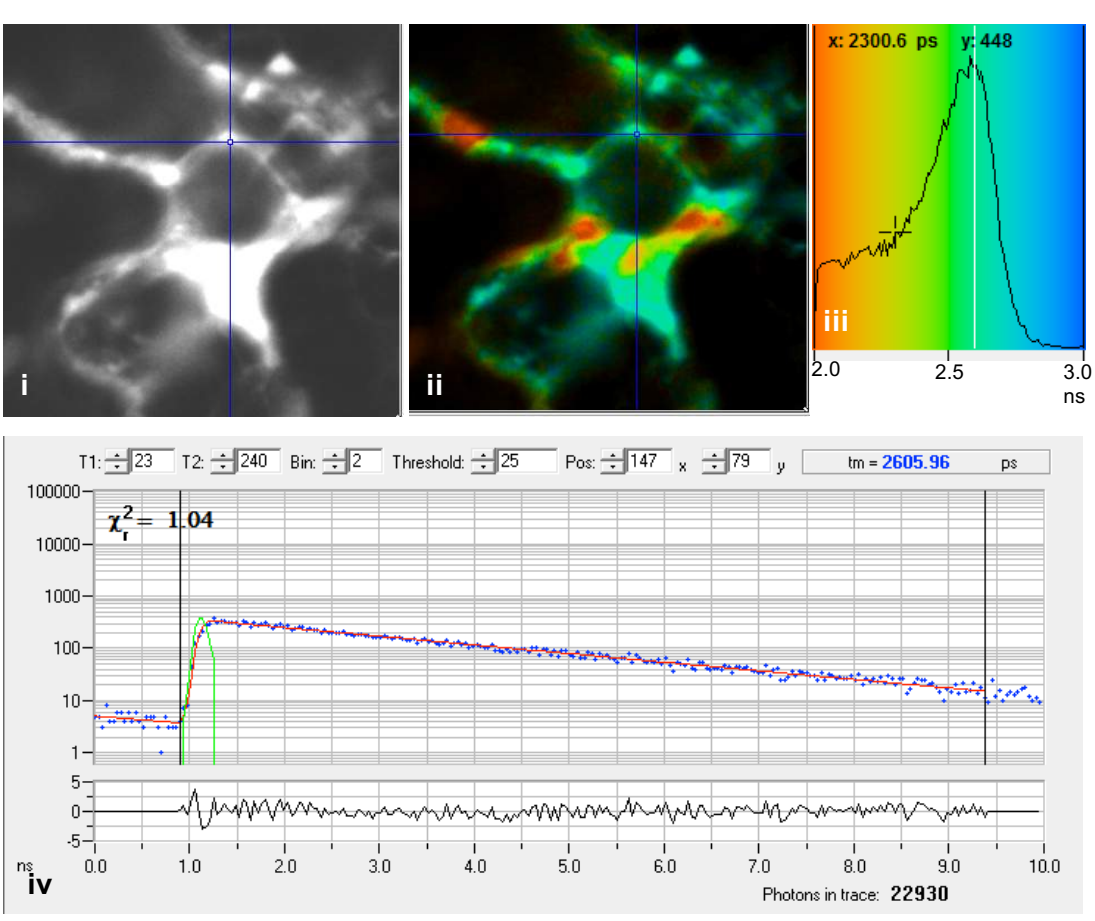

Supplemental Table 1. Oligonucleotide primers used for the generation of the RTN13 constructs in this study.

Purpose	Primer Name	Sequence
attB PCR product for YFP:RTN13	YFP:RTN13 LP (Gateway)	AAAAAAGCAGGCTTCATGGTGAGCAAGGGCGAGGAGCTG
	YFP:RTN13 RP (Gateway)	CAAGAAAGCTGGGTCCTACTCTGATTTTTTCACTTTCTCTTCTGTACC
installing full length attB sites	attB1 adaptor	GGGGACAAGTTTGTACAAAAAAGCAGGCT
	attB2 adaptor	GGGGACCACTTTGTACAAGAAAGCTGGGT
XbaI:YFP:RTN13:SacI	YFP:RTN13 LP (RE cloning)	CAGATATCTAGAATGGTGAGCAAGGGCGAGGAGCTG
	YFP:RTN13 RP (RE cloning)	CAGATAGAGCTCCTACTCTGATTTTTTCACTTTCTCTTCTGTACC
Sequencing inserts	pVKH18-En6 LB	CCTTCGCAAGACCCTTCCTC
	pVKH18-En6 RB	CATGCAAGACCGGCAACAG
SDM of YFP:RTN13 pDONRZeo to generate YFP:RTN13 I165K	YFP:RTN13 I165K LP	GGAGATCAAAAGCAGAAGCATTTGGGTAGCC
	YFP:RTN13 I165K RP	GTACTCTTCCCACAACTTTGGAACCGTCAACC
XbaI:YFP:RTN13ΔAPH:SacI (insertion of STOP codon after residue E159)	YFP:RTN13 LP (RE cloning)	CAGATATCTAGAATGGTGAGCAAGGGCGAGGAGCTG
	YFP:RTN13ΔAPH+C RP (RE cloning)	CAGATAGAGCTCCTATTCCCACAACTTTGGAACCGTCAACC
Deletion of APH (E160-L169)	YFP:RTN13ΔAPH LP1	CGGTTCCAAAGTTGTGGGAAGGTAGCCTTAAAGATAAATCGAAGGG
	YFP:RTN13ΔAPH RP1	CCCTTCGATTTATCTTTAAGGCTACCTTCCCACAACTTTGGAACCG
Deletion of APH (G170-K175)	YFP:RTN13ΔAPH LP2	CGGTTCCAAAGTTGTGGGAATCGAAGGGAGCGT
	YFP:RTN13ΔAPH RP2	ACGCTCCCTTCGATTCCCACAACTTTGGAACCG
mCh:RTN13 Fusion PCR. mCherry fragment	mCherry LP (RE cloning)	CAGATATCTAGAATGGTGAGCAAGGGCGAGGA
	mCherry:RTN13 RP (RE cloning)	TGGATCTTTGGTCACGTCGTTGGCCTTGTACAGCTCGTCCATGC
mCh:RTN13 Fusion PCR. RTN13 fragment	mCherry:RTN13 LP (RE cloning)	GCATGGACGAGCTGTACAAGGCCAACGACGTGACCAAAGATCCA
	YFP:RTN13 RP (RE cloning)	CAGATAGAGCTCCTACTCTGATTTTTTCACTTTCTCTTCTGTACC